IEEE Photonics Journal
An IEEE Photonics Society Publication

Open Access

# Chaos Suppression and Phase Locking in an Nd:$YVO_4$ Laser by Reshaping Pump Modulation With Dual Waveforms

Volume 5, Number 1, February 2013

**Ken-Chia Chang**
**Ming-Dar Wei**

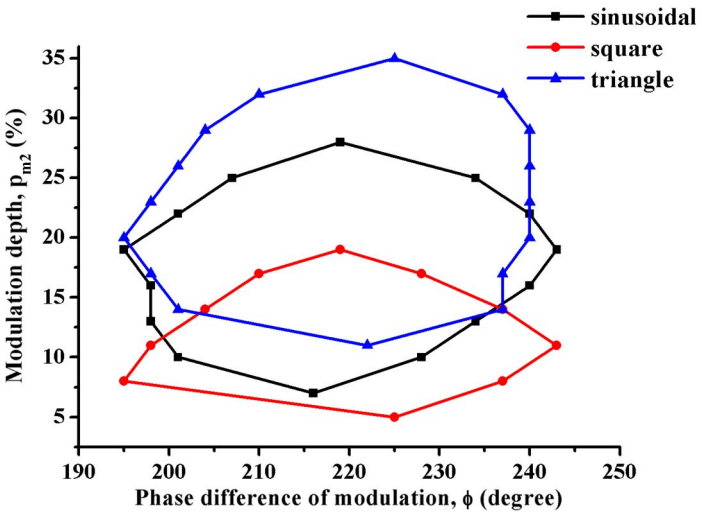


DOI: 10.1109/JPHOT.2012.2235420
1943-0655/$31.00 ©2012 IEEE

IEEE photonics SOCIETY

IEEE

# Chaos Suppression and Phase Locking in an Nd:$YVO_4$ Laser by Reshaping Pump Modulation With Dual Waveforms

**Ken-Chia Chang and Ming-Dar Wei**

Department of Photonics, National Cheng Kung University, Tainan City 70101, Taiwan

*DOI: 10.1109/JPHOT.2012.2235420*
*1943-0655/$31.00 ©2012 IEEE*

Manuscript received November 30, 2012; accepted December 15, 2012. Date of publication December 19, 2012; date of current version February 1, 2013. This work was supported by the National Science Council of the Republic of China under Contracts NSC 101-2112-M-006-014-MY3. Corresponding author: M.-D. Wei (e-mail: mdwei@mail.ncku.edu.tw).

**Abstract:** This paper demonstrated the suppression of chaos in an Nd:$YVO_4$ laser by reshaping the pump modulation with dual waveforms. When the first sinusoidal modulation induced chaos, the second modulated signal reshaped the modulated profile to suppress the chaos. A chaos-suppressed route associated with double phase locking was observed as the modulation depth of the second modulation increased; the first phase locking accompanied the subharmonic oscillation of the output intensity, and the second phase locking regenerated the chaos. Varying the waveforms of the second modulation to be square, triangle, and sinusoidal reshapes the modulated profile to change the suppression region; therefore, the shape can be used as a parameter to control the dynamics. Numerical simulations were confirmed by the experimental results.

**Index Terms:** Chaos, solid-state laser, diode-pumped laser.

## 1. Introduction

Chaos control or suppression has attracted considerable interest since Ott et al. first demonstrated the control of chaos [1]. Various chaos control schemes have been proposed in subsequent studies, including feedback and nonfeedback schemes [2]. Nonfeedback control is based mainly on the periodic excitation of the system. Chacón recently indicated that geometrical resonance provides the mechanism underlying the nonfeedback control of chaos based on a dynamic system under biharmonic modulation [3]. The initial phase of second harmonic perturbation plays a vital role in the suppression and enhancement of chaos in nonautonomous systems [4]. For lasers, the second subharmonic modulation suppressing chaotic behavior induced by a modulation mechanism was observed in a modulated microchip $LiNdP_4O_{12}$ laser [5]. The phase differences in biharmonic modulation were observed in a $CO_2$ laser [6], [7]. The crucial role of the initial phase difference was verified in an Nd:$YVO_4$ laser with biharmonic pump modulation [8].

Moreover, the dynamic behavior is affected by the shape of the modulation or perturbation [9]–[12]. Because the solutions of several nonlinear oscillators are provided for Jacobian elliptic functions, modulations with Jacobian elliptic functions can be used to examine the reshaping-induced dynamics [9]. A reshaping modulation profile was used to examine the dynamics in a damped-driven Helmholtz oscillator [10] and in damped sine-Gordon systems [11]. The nonlinear dynamics of a single-mode bidirectional solid-state ring laser were explored under the influence of square-wave modulation [12]. The role of reshaping the modulation profile in a modulated system under dual waveforms is crucial.

We examined the suppression of chaos in an Nd:$YVO_4$ laser with a biwaveform pump modulation, in which the first modulation for chaos induction was sinusoidal, and the second modulation for chaos suppression was square, triangle, and sinusoidal. The initial phase difference of these two modulated signals and modulation depths, defined as the modulation amplitude divided by the average value of the pump intensity, determined the region of the suppressing chaos [8]. The profile of the second modulation altered the region of the suppressing chaos. Moreover, phase locking induced specific dynamic behavior in the suppression region. The experimental results support the suppression of chaos.

## 2. Modeling

Based on the approach by Fox and Li [13], an iterative method has been widely used to explore laser systems. In solid-state lasers, the iterative method has been applied to determine the cavity decay rate and relaxation oscillation frequency [14], the cavity-configuration-dependent instability [8], [15], [16] in CW lasers, the mode parameters [17] and chaos [18] in Q-switched lasers, and the chaos in Kerr-lens mode-locked lasers [19]. By using an Nd:YAG laser, Cheng et al. established a model based on the coupled equations of the rate equation and the generalized Huygens diffraction integral to analyze the cavity decay rate and relaxation oscillation frequency in unconventional laser cavities [14]. Because the standing wave cavity configuration can be unfolded into an equivalent lens guide system, the laser can be characterized with reference to a cascading propagation of the optical field in the gain medium and the cold cavity. The rate equation represents the propagation of an electric field through the gain medium that is lumped into a single gain sheet, and the generalized Huygens diffraction integral with the round-trip ABCD matrix [20] describes the propagation of the optical field in the cold cavity. Similar coupled equations were used to examine the chaotic behavior in a solid-state laser [21] and in subsequent studies [8], [15], [16]. Because a solid-state laser is a class-B laser, the equations associated with the population inversion and with the electric field dominate the laser dynamics. The generalized Huygens diffraction integral, used to describe the variation of the electric field, can easily consider the contribution of the cavity mode and the coupling between the pump and cavity distributions. Thus, the model has the advantages of detailing the transverse distribution and the cavity-configuration-dependent characteristics.

According to earlier works [14]–[16], the optical fields $E_n$ and the population inversion $N_n$, where the index n denotes the number of iterations and corresponds to the nth round trip, are governed by

$$E_n^+(r) = \rho E_n^-(r)\exp[\sigma \Delta N_n(r) d] \tag{1}$$

$$E_{n+1}^-(r) = -\frac{2\pi i}{\lambda B} e^{i2kL} \int E_n^+(r')\exp\left[-\frac{i\pi}{\lambda B}(Ar'^2 + Dr^2)\right] J_0\left(\frac{2\pi r r'}{\lambda B}\right) r' dr' \tag{2}$$

$$\Delta N_{n+1}(r) = \Delta N_n(r) + R_n(r)\Delta t - \gamma \Delta N_n(r)\Delta t - \gamma\left(\left|E_n^-(r)\right|^2 / E_s^2\right)\Delta N_n(r)\Delta t \tag{3}$$

where r and r′ are the corresponding radial coordinates; $R_n$ is the pumping rate; $\gamma$ is the spontaneous decay rate; $\rho$ is the reflective coefficient of the output coupled mirror; $\sigma$ is the stimulated emission cross section; d is the length of the gain medium; $\lambda$ is the wavelength of the laser; k is the wavenumber; L is the length of one round trip; A, B, and D are the elements of the ABCD matrix; $\Delta t$ is the travel time through the gain medium; and $J_0$ is the Bessel function of zero order. $E_s$ is the saturation intensity determined by $\gamma$ and $\sigma$. Superscripts $+$ and $-$ refer to after and before the gain medium, respectively. An Nd:$YVO_4$ laser with a plano-concave cavity was examined. The parameters of the laser are $\sigma = 2.5 \times 10^{-18}$ cm$^2$ and $1/\gamma = 50$ $\mu$s, and the reflectivity of the output coupler is 90%. The cavity length was $L = 59$ mm with the cavity g-parameters [20] having $g_1 g_2 = 0.2625$.

Considering a biwaveform pump modulation, the pumping rate must be represented as

$$R_n(r) = R_{pm}(r)[1 + p_{m1}\sin(2\pi f_{m1} n t_r) + p_{m2} wf(2\pi f_{m2} n t_r + \phi)] \tag{4}$$

where $t_r$ is the roundtrip time, $f_{mi}$ is the modulation frequency, and $p_{mi}$ is the modulation depth defined as the modulation amplitude of intensity divided by the average intensity for the pump laser. The indexes $i = 1$ and $i = 2$ refer to the quality of the signals generated from the first and second

modulations, respectively. The spatial distribution of the pumping rate $R_{pm}$ was set to the Gaussian profile. This paper considered a spot size with a pump beam of 300 $\mu$m at P = 1 W. The relation between the pump power P and pumping rate is shown in [15]. The modulation frequency of the first modulation resonated with the relaxation oscillation frequency to induce chaos. The sinusoidal wave was selected as the first modulation because suppression of chaos that resulted from the second modulation was the focus of this paper. The term $wf(2\pi f_{m2}t + \phi)$ indicates that the second modulation was an arbitrarily periodic waveform with a frequency of $f_{m2}$ and had the initial phase difference $\phi$ to the first modulation. Square, triangular, and sinusoidal waveforms were chosen to examine the chaos suppression according to the modulation shape. The mixed waveform will be periodic only if $f_{m1}/f_{m2}$ is rational. The frequencies were set to $f_{m2} = f_{m1}/2$ in the following discussions. Varying $p_{m2}$ and $\phi$ reshapes the sinusoidal waveform generated by the first modulation to suppress the chaotic behavior.

## 3. Numerical Simulations

In a single-modulation system, a period-doubling route to chaos was first observed experimentally when the modulation frequency approached the relaxation oscillation frequency of the laser and when the modulation depth exceeded a bifurcating threshold [22]. Based on this model, a bifurcation diagram in the numerical simulation was shown in [23, Fig. 3]. The bifurcation was dominated by period doubling; however, differences exist to the typical period-doubling route. The oscillations show periods 1 and 2 alternating with the modulation depth in the region varying between 2.0% and 2.5%. The system switches back and forth between periods 1 and 2 in the experiments. After the period-4 evolution, the route shows that each peak intensity fluctuation rises as increases the modulation depth, and the evolution merges to become chaotic. A high period such as period 8 exists, but the region in the dynamical parameter of the modulation depth is unclear. This phenomenon may be due to the coupling of the transverse (radial) electric distribution in (2) to complicate the dynamics. The numerical results agree with that only the first two bifurcations could be resolved in the experiment [22].

The threshold of the modulation depth for chaotic behavior is $p_{m1} = 3.83\%$ at a relaxation oscillation frequency of 772 kHz. We set $p_{m1} = 4.596\%$, which was 1.2 times the threshold, to operate at a chaotic output. Fig. 1 shows the characteristic analysis of this chaotic signal. The chaotic intensity output and a broadened spectrum obtained by fast Fourier transform (FFT) are shown in Fig. 1(a) and (b), respectively. Using the time-embedding technique to reconstruct the trajectory from the time series to quantitatively determine the fractal characteristic of the nonlinear dynamic attractor, the correlation dimension using Grassberger–Procaccia analysis (GPA) [24], [25] was calculated, and it is shown in Fig. 1(c). The commercial chaos data analyzer (CDA) from the American Institute of Physics was used to analyze the data. The correlation dimension reaches a constant when the embedding dimension is sufficiently large to accommodate the attractor. The correlation dimension is approximately 3.491, which is the average value of an embedding dimension of 7 to 10. Further, false nearest neighbors (FNN) [26] analysis could help establish the chaotic nature of the signal and discriminate it from noise. Fig. 1(d) shows the results of FNN analysis regarding the chaotic data, revealing a rapid fall to zero at a low embedding dimension of approximately four. A low-dimension deterministic chaos was achieved as the first modulation was added with $p_{m1} = 4.596\%$.

In this paper, the system was added the second modulation and $f_{m2} = 386$ kHz to explore the laser dynamics. Fig. 2 shows the regions of chaos suppression achieved by varying $p_{m2}$ and $\phi$ simultaneously when the second modulated waveform was square. Chaos can be suppressed to be periodic within a closed region. The initial phase and modulation depth of the second-harmonic perturbation must satisfy specific conditions to achieve chaos suppression. Because the addition of the second modulation reshapes the waveform of the pump laser under a subharmonic frequency, the dynamics depended on the shape of the modulation waveform [8].

Within the periodic region, most of the output intensity oscillated at an average frequency of $f_{m1}$. However, subharmonic oscillation occurred near the central initial phase of the suppressed region.

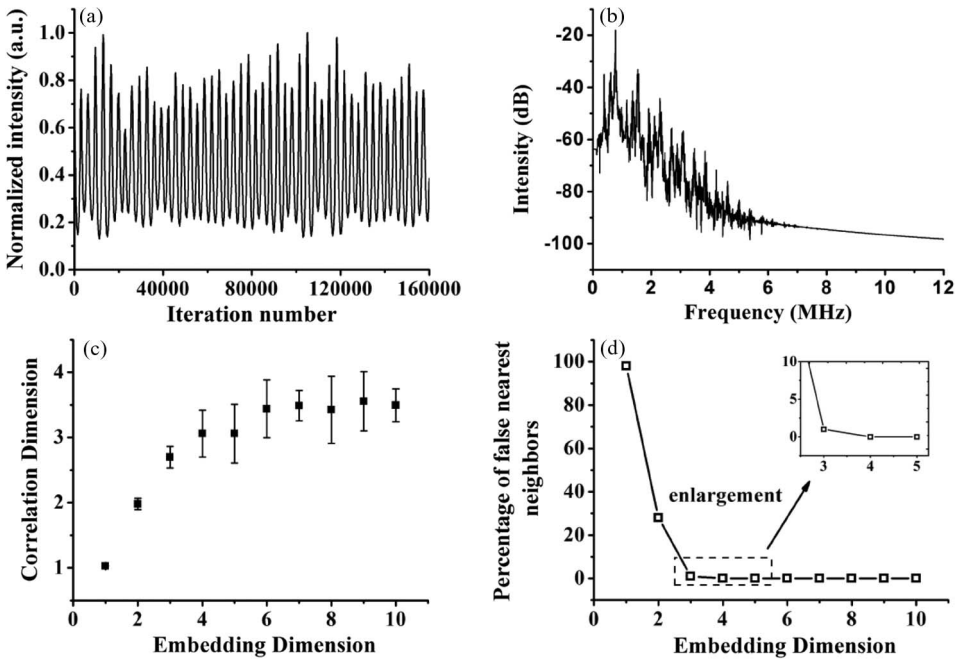


Fig. 1. Analyses of the chaotic signal with $p_{m1} = 4.596\%$ and $p_{m2} = 0$ relating to (a) Intensity and (b) spectrum, and the (c) correlation dimension and (d) false nearest neighbors versus the embedding dimension.

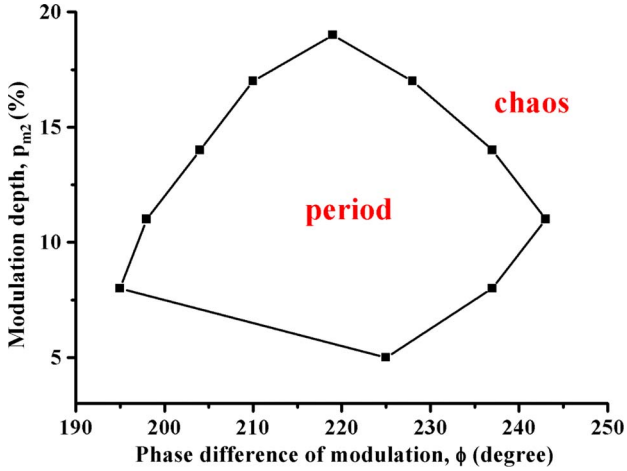


Fig. 2. Boundary of chaos-suppressed region with the second modulation being square. A periodic intensity was obtained inside the closed region.

Fig. 3(a) shows the average frequency and the phase difference as a function of $p_{m2}$ with the square second modulation and $\phi = 219°$. The phase of the output intensity can be computed using Hilbert transform, and fitting the slope in the phase versus time yields the average frequency [27]. Based on the Hilbert transform, the local maximal intensity corresponds to the phase of $2\pi q$, where q is an integer. Thus, the phase difference between the pump and output lasers, i.e., $\Phi$, was determined by the difference of the phase between the corresponding maximal intensity of output laser and that of the pump laser, as labeled in Fig. 3(b). When $p_{m2}$ was less than 6%, the system

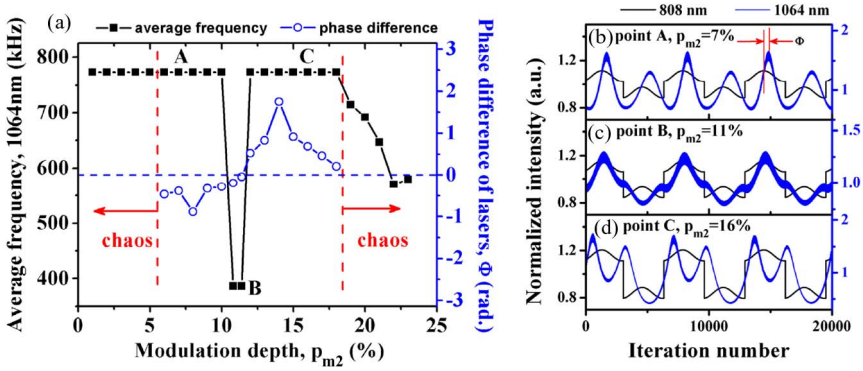


Fig. 3. (a) The average frequency and the phase difference as a function of $p_{m2}$ at $\phi = 219^o$ with solid-square and circle symbols, respectively. The right column shows the time evolution at various $p_{m2}$'s with (b) 7%, (c) 11%, and (d) 16%.

remained chaotic. The average frequency approached the modulation frequency of the first modulation, although the instantaneous frequency fluctuated because of the chaos. Because the output intensity was chaotic, no fixing phase difference occurred between the pump and output intensities, and no related data are shown in Fig. 3(a). The first modulation frequency resonating to the relaxation oscillation frequency dominated the chaotic behavior in this region. Continuing to increase $p_{m2}$, chaos was suppressed, as shown in Fig. 3(b) with $p_{m2} = 7\%$, and the average frequency was still locked to $f_{m1}$. The output intensity lagged behind the pump intensity because of a minus phase difference. The average frequency decreased abruptly to $f_{m2} = f_{m1}/2 = 386$ kHz when $p_{m2}$ was approximately 11%. The phase difference was approximately zero; that is, phase locking occurred. This subharmonic oscillation region emerged with a phase difference $\phi$ of $218^o \pm 1^0$ and $p_{m2}$ of 11.1% ± 0.3%. A comparison in Fig. 3(b) and (c) shows that high-peak and low-peak oscillation amplitudes formed a typical oscillation in the suppression region, such as $p_{m2} = 7\%$; however, the low-peak oscillation was suppressed as phase locking, as shown in Fig. 3(c). When $p_{m2}$ was greater than it is in the phase-locked region, the output profile split into two humps, as shown in Fig. 3(d), and a positive phase difference occurred. The phase difference, which was increasing, start decreasing when $p_{m2}$ was greater than 13%. Finally, second-time phase locking formed, and the system became chaotic again at $p_{m2} = 19\%$. In contrast to the region with $p_{m2} < 6\%$, the average frequencies of the chaotic intensities transferred gradually from $f_{m1}$ to $f_{m2}$. Although a mixed contribution of two modulations excited the chaotic behavior, the subharmonic modulation gradually dominated the dynamics. A route of suppression chaos was associated with phase locking that occurred twice.

This paper further explored the dynamics under various reshaping waveforms. Fig. 4 shows the regions of chaos suppression achieved by varying $p_{m2}$ and $\phi$ simultaneously when the second modulated waveforms were sinusoidal, square, and triangular, and they are respectively represented by the solid square, circle, and triangle symbols. The chaotic dynamics originally excited by the first modulation were suppressed to be periodic within the closed region. The suppressed regions moved toward the high $p_{m2}$ when the shapes of the second modulation were square, sinusoidal, and triangular. The reshaping modulation can be considered the sum of the harmonic modulations based on the expansion of the Fourier series. For example, the square wave with the frequency $f_{m2}$ and unit amplitude can be expanded as [28]

$$x_{square}(t) = \frac{4}{\pi}\sum_{k=1}^{\infty}\frac{\sin[2\pi(2k-1)f_{m2}t]}{(2k-1)} = \frac{4}{\pi}\left[\sin(2\pi f_{m2}t) + \frac{1}{3}\sin(6\pi f_{m2}t) + \frac{1}{5}\sin(10\pi f_{m2}t)\ldots\right]. \quad (5)$$

Because the first expansion term of the square wave from (5) has a factor of $4/\pi$, the modulation depth in the square wave is equivalent to $4/\pi$ times the modulation depth in the sinusoidal wave if

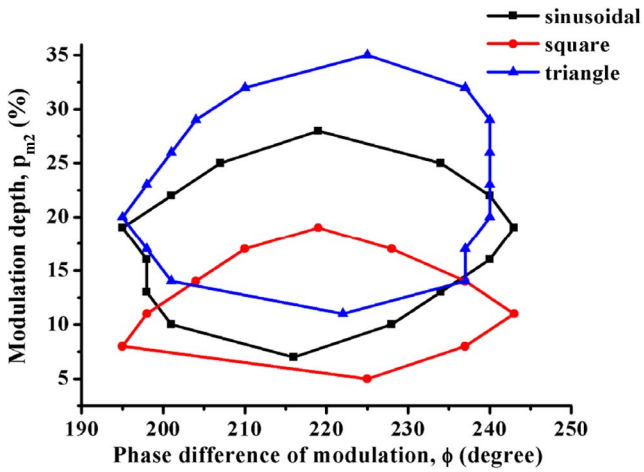


Fig. 4. Boundaries of chaos-suppressed regions with various modulation shapes of the second modulations. A periodic intensity was observed inside each region.

only the first term is considered. Thus, low modulation depth can suppress the chaos in square-wave modulation. However, the suppressed region of the sinusoidal-wave modulation does not shift by a factor of $4/\pi$. Thus, considering that the shape is equivalent is considering all nonlinear harmonic resonance with suitable weights. Similarly, the high modulation depth can suppress the chaos in triangle-wave modulation, in which the first expansion term of the triangle has a factor of $8/\pi^2$. In addition to the modulation depth and the phase difference in biwaveform modulation, the shape can be a tunable parameter in modulation systems and be equivalent to multiharmonic modulations to excite or control the dynamics simultaneously.

The route of chaos suppression associated with double phase locking also occurred in systems with triangular and sinusoidal modulations. The subharmonic oscillation regions for the triangular and sinusoidal modulations were $214.5^o \pm 1.5^o$ and $216.0^o \pm 3.0^0$, respectively, in the phase difference $\phi$, and 22.5% $\pm$ 1.5% and 16.5% $\pm$ 1.5% in $p_{m2}$, respectively. Because the initial phase is dominated mainly by the ratios of $f_{m1}$ and $f_{m2}$, the values were close for various shapes. The phase difference of the modulations exhibited a small shift, which may be attributed to the effects of the high harmonic oscillation.

## 4. Experimental Results

The numerical results were further verified by the experiments. Fig. 5(a) shows the experimental setup. A simple plano-concave Nd:$YVO_4$ laser was pumped by a diode laser with a wavelength of 808 nm and a maximal output power of 1 W. The Nd:$YVO_4$ crystal had dimensions of $3 \times 3 \times 1$ $mm^3$ and 1 at.% $Nd^{3+}$ doping. One side of the Nd:$YVO_4$ crystal had an antireflection coating at 808 nm and a highly reflective coating at 1064 nm to serve as a cavity mirror. A concave mirror with a radius of curvature of $R_c = 80$ mm and a reflectivity of 90% was used as the mirror at the other end and the output coupler. The signal of the intensity was measured using a high-speed photodetector with an oscilloscope. Two function generators injected the signal to the diode laser to generate the pump modulation. A cavity length of 60.6 mm was determined by the beating frequency of longitudinal modes to yield $g_1 g_2 = 0.2625$. The relaxation oscillation frequency was 470 kHz; thus, $f_{m1} = 470$ kHz and $f_{m2} = 235$ kHz. Fig. 5(b) displays that the evolution of the output intensity is chaotic when $p_{m1} = 6.21\%$ and $p_{m2} = 0$. The correlation dimension using the Grassberger–Procaccia analysis is 3.574, as shown in Fig. 5(c). The embedding dimension using FNN analysis is approximately four. The experimental results agree with numerical simulations.

Fig. 6 shows the regions of chaos suppression by simultaneously varying $p_{m2}$ and $\phi$ when the second modulated waveforms are sinusoidal, square, and triangular, which are represented by the

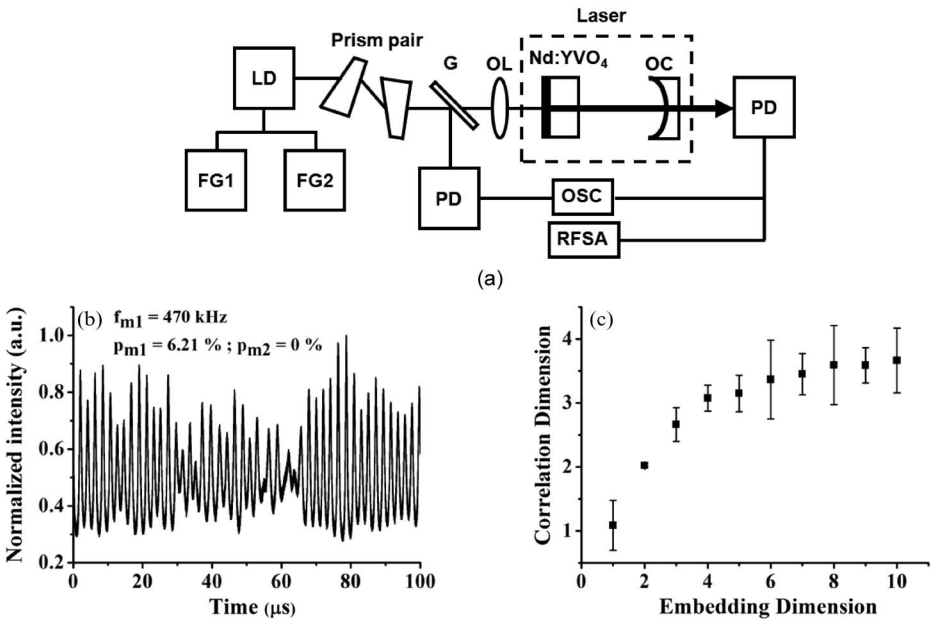


Fig. 5. (a) The experimental setup: OL, objective lens; OC, output coupler; PD, photodetector; LD, laser diode; FG1 and FG2, function generator 1 and 2; OSC, oscilloscope; RFSA, RF spectrum analyzer. (b) A chaotic intensity was obtained when $p_{m1} = 6.21\%$ and $p_{m2} = 0$, i.e., a case of single modulation, and (c) The correlation dimension as a function of embedding dimension was demonstrated.

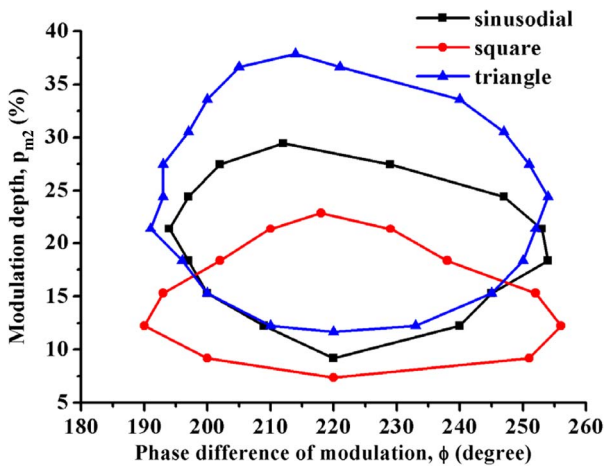


Fig. 6. Boundaries of chaos-suppressed regions with various modulation shapes of the second modulations. A periodic intensity was observed inside each region.

solid square, circle, and triangle symbols, respectively. The suppression behavior was strongly determined by the initial phase $\phi$, and the suppressed regions depended on the modulation shape. Consistent with the numerical results, the suppression region had a higher $p_{m2}$ for triangular modulation and a lower $p_{m2}$ for the square modulation than that of sinusoidal modulation, and the central phase difference between two modulations was approximately $\phi = 220^o$. The phase locking to subharmonic oscillation and chaos was also generated at a specific modulation depth of the second modulation, as shown in Fig. 7(a), with $\phi = 220^o$; the intensities at various modulation depths are shown in Fig. 7(b)–(d). The experimental results were consistent with those of the numerical simulations.

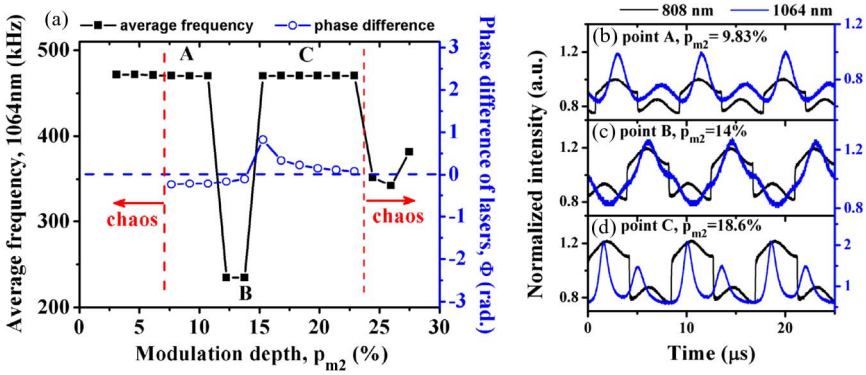


Fig. 7. (a) The average frequency and the phase difference as a function of $p_{m2}$ at $\phi = 220^{o}$ with solid-square and circle symbols, respectively. The right column shows the time evolution at various $p_{m2}$'s with (b) 9.83%, (c) 14%, and (d) 18.6%.

## 5. Conclusion

This paper has investigated chaos suppression in an Nd:$YVO_4$ laser by modulating a pump using dual waveforms. The modulation frequency of the first waveform has been adjusted to be close to the relaxation oscillation frequency, and the laser typically behaves chaotically when the modulation depth increases to a specific threshold. However, chaos can be suppressed by adding a second modulation to reshape the waveform of the pump laser under a subharmonic frequency, in which the shapes of the second modulations are square, sinusoidal, and triangular. The suppression region varies depending on the initial phase and the modulation depth of the second modulation because of the various reshaping waveforms. A chaos-suppressed route associated with double phase locking was observed as the modulation depth of the second modulation increased; the first phase locking accompanied the subharmonic oscillation of the output intensity, and the second phase locking regenerated the chaos. The experimental results are consistent with the numerical simulations.

## References

[1] E. Ott, C. Grebogi, and J. A. Yorke, "Controlling chaos," *Phys. Rev. Lett.*, vol. 64, no. 11, pp. 1196–1199, Mar. 1990.
[2] T. Kapitaniak, *Controlling Chaos: Theoretical and Practical Methods in Non-linear Dynamics*. San Diego, CA: Academic, 1996.
[3] R. Chacón, "Geometrical resonance as a chaos eliminating mechanism," *Phys. Rev. Lett.*, vol. 77, no. 3, pp. 482–485, Jul. 1996.
[4] R. Chacón, "Maintenance and suppression of chaos by weak harmonic perturbation: A unified view," *Phy. Rev. Lett.*, vol. 86, no. 9, pp. 1737–1740, Feb. 2001.
[5] K. Otsuka, J.-L. Chern, and J.-S. Lih, "Experimental suppression of chaos in a modulated multimode laser," *Opt. Lett.*, vol. 22, no. 5, pp. 292–294, Mar. 1997.
[6] V. N. Chizhevsky, R. Corbalán, and A. N. Pisarchik, "Attractor splitting induced by resonant perturbations," *Phys. Rev. E, Stat., Nonlin., Soft, Matter Phys.*, vol. 56, no. 2, pp. 1580–1584, Aug. 1997.
[7] I. B. Schwartz, I. Triandaf, R. Meucci, and T. W. Carr, "Open-loop sustained chaos and control: A manifold approach," *Phys. Rev. E, Stat., Nonlin. Soft Matter Phys.*, vol. 66, no. 2, p. 026213, Aug. 2002.
[8] M.-D. Wei, C.-C. Hsu, H.-H. Huang, and H.-H. Wu, "Chaos suppression in a Nd:$YVO_4$ laser by biharmonical pump modulation," *Opt. Exp.*, vol. 18, no. 19, pp. 19 977–19 982, Sep. 2010.
[9] R. Chacón, *Control of Homoclinic Chaos by Weak Periodic Perturbations*. Singapore: World Scientific, 2005.
[10] F. Balibrea, R. Chacón, and M. A. López, "Reshaping-induced order-chaos routes in a damped driven Helmholtz oscillator," *Chaos Solitons Fractals*, vol. 24, no. 2, pp. 459–470, Apr. 2005.
[11] R. Chacón, "Reshaping-induced spatiotemporal chaos in driven, damped sine-Gordon systems," *Chaos Solitons Fractals*, vol. 31, no. 5, pp. 1265–1271, Mar. 2007.
[12] F. Rawwagah and S. Singh, "Nonlinear dynamics of a modulated bidirectional solid-state ring laser," *J. Opt. Soc. Amer. B, Opt. Phys.*, vol. 23, no. 9, pp. 1785–1792, Sep. 2006.
[13] A. G. Fox and T. Li, "Resonant modes in a maser interferometer," *Bell Syst. Tech. J.*, vol. 40, pp. 453–458, Mar. 1961.
[14] Y. P. Cheng, P. L. Mussche, and A. E. Siegman, "Cavity decay rate and relaxation oscillation frequency in unconventional laser cavities," *IEEE J. Quantum Electron.*, vol. 31, no. 2, pp. 391–398, Feb. 1995.

[15] C.-H. Chen, M.-D. Wei, and W.-F. Hsieh, "Beam-propagation-dominant instability in an axially pumped solid-state laser near degenerate resonator configurations," *J. Opt. Soc. Amer. B*, vol. 18, no. 8, pp. 1076–1083, Aug. 2001.
[16] M.-D. Wei, C.-H. Chen, H.-H. Wu, D.-Y. Huang, and C.-H. Chen, "Chaos suppression in the transverse mode degeneracy regime of a pump-modulated Nd:$YVO_4$ laser," *J. Opt. A, Pure Appl. Opt.*, vol. 11, no. 4, p. 045504, Apr. 2009.
[17] J. K. Jabczynski, J. Kwiatkowski, and W. Zendzian, "Modeling of beam width in passively Q-switched end-pumped lasers," *Opt. Exp.*, vol. 11, no. 11, pp. 552–559, Mar. 2003.
[18] M. Kovalsky and A. Hnilo, "Chaos in the pulse spacing of passive Q-switched all-solid-state lasers," *Opt. Lett.*, vol. 35, no. 20, pp. 3498–3500, Oct. 2010.
[19] M. G. Kovalsky and A. A. Hnilo, "Different routes to chaos in the Ti:sapphire laser," *Phys. Rev. A, At., Mol., Opt. Phys.*, vol. 70, no. 4, p. 043813, Oct. 2004.
[20] A. E. Siegman, *Lasers*. Herndon, VA: Univ. Sci. Books, 1986.
[21] F. Hollinger and C. Jung, "Single-longitudinal-mode laser as a discrete dynamical system," *J. Opt. Soc. Amer. B, Opt. Phys.*, vol. 2, no. 1, pp. 218–225, Jan. 1985.
[22] W. Klische, H. R. Telle, and C. O. Weiss, "Chaos in a solid-state laser with a periodically modulated pump," *Opt. Lett.*, vol. 9, no. 12, pp. 561–563, Dec. 1984.
[23] M.-D. Wei and C.-C. Hsu, "Reshaping modulation profile to increase and decrease the threshold for chaotic behavior in a pump-modulation Nd:$YVO_4$ laser," *Int. J. Bifurcation Chaos*, vol. 22, no. 8, p. 1250185, Aug. 2012.
[24] P. Grassberger and I. Procaccia, "Characterization of strange attractors," *Phys. Rev. Lett.*, vol. 50, no. 5, pp. 346–349, Jan. 1983.
[25] A. Ben-Mizrachi, I. Procaccia, and P. Grassberger, "Characterization of experimental (noisy) strange attractors," *Phys. Rev. A, At., Mol., Opt. Phys.*, vol. 29, no. 2, pp. 975–977, Feb. 1984.
[26] M. B. Kennel, R. Brown, and H. D. I. Abarbanel, "Determining embedding dimension for phase-space reconstruction using a geometrical construction," *Phys. Rev. A, At., Mol., Opt. Phys.*, vol. 45, no. 6, pp. 3403–3411, Mar. 1992.
[27] Y.-C. Lai and N. Ye, "Recent developments in chaotic time series analysis," *Int. J. Bifurcation Chaos*, vol. 13, no. 6, pp. 1383–1422, Jun. 2003.
[28] E. Kreyszig, *Advance Engineering Mathematics*. New York: Wiley, 2011.